Journal of Electroanalytical Chemistry 850 (2019) 113380

Contents lists available at ScienceDirect

Journal of Electroanalytical Chemistry

journal homepage: www.elsevier.com/locate/jelechem

Structural modifications and ionic transport of PVA-KOH hydrogels applied in Zn/Air batteries

Florencio Santos [a], Juan P. Tafur [a,b], José Abad [a], Antonio J. Fernández Romero [a,*]

[a] Grupo de Materiales Avanzados para la Producción y Almacenamiento de Energía, Universidad Politécnica de Cartagena, Aulario II, Campus de Alfonso XIII, 30203 Cartagena, Spain
[b] School of Chemical Science and Engineering, Yachay Tech University, Yachay City of Knowledge, 100650 Urcuqui, Ecuador

ARTICLE INFO

Article history:
Received 8 April 2019
Received in revised form 17 July 2019
Accepted 12 August 2019
Available online 28 August 2019

Keywords:
Polymer electrolyte
Ionic conductivity
PVA
Grothuss mechanism
Zinc/Air battery

ABSTRACT

A series of Poly (vinyl alcohol) (PVA)-based gel polymer electrolytes doped with KOH solution have been synthesized by a cast method in absence of other additives and crosslinkers. Immersion of these membranes in 12 M KOH solution causes the entrance of a higher amount of KOH and water inside the polymeric matrix. XRD, TGA, XPS and ATR-FTIR measurements confirm PVA chains restructure depending on the amount of KOH and water inside the membrane. This fact is in agreement with the improvement of the ionic conductivity, diminishing of activation energy and increasing of peaks intensities in cyclic voltammograms. Besides, these PVA-KOH membranes have been tested in Zn/PVA-KOH/Air batteries confirming the importance of the amount of KOH and water inside the gel polymer electrolyte. Finally, XRD and EDX measurements demonstrate the confinement of Zn^{++} close to Zn electrode during the test of Zn/Air batteries, making necessary the movement of OH^- anions inside the membrane, as the only ionic species causing the charge transport through the membrane. This fact, together with spectroscopic and electrical results allows us to discuss the improvement of the anionic transport inside the membranes based on the Grotthuss mechanism.

1. Introduction

Gel polymer electrolytes (GPEs) are materials which are neither solids nor liquids but hold both the cohesive properties of solids and the diffusive character of liquids. Hence, these electrolytes have become relevant due to their use as excellent substitutes of the liquid electrolytes or as separators in ionic devices including batteries, super-capacitors, fuel cells, and others [1–4]. GPEs can be prepared by trapping liquid electrolytes into different polymer hosts. In this case, the salt provides free-mobile ions which take part in the conduction process; the plasticizing solvent allows to increase the conductivity values in GPEs due to the ions solvating, and the polymer provides mechanical stability. Hence, the morphology and properties of GPEs will depend on the type and the amount of polymer host, salt and solvent present in the polymer matrix. [3–19].

The use of a GPE in a battery needs to fulfil some requirements, such as high ionic conductivity and good mechanical and electrochemical stabilities at a wide temperature range [11]. There are numerous previous studies using different polymer as host material, including polyethylene oxide (PEO), polyacrylonitrile (PAN), polymethylmethacrylate (PMMA) and, poly (vinylidene fluoride-*co*-hexafluoropropylene) (PVdF-HFP) to name but a few, which have been tested in different battery types [11–19]. However, among biodegradable synthetic polymer, polyvinyl alcohol (PVA) is a promising candidate material to become the polymer host due to its ability to provide good optical, mechanical and electrochemical properties. PVA is also a semi-crystalline polymer with high hydrophilicity, easy to prepare, non-toxic and cheap material.

PVA doped with potassium hydroxide (KOH) has been studied extensively and received much attention due to their wide application in electrochemical devices such as super-capacitors, anion exchange membranes for fuel cells and Zinc alkaline batteries [4–10].

KOH is incorporated to the PVA to provide free ions mobiles inside the membrane. However, the addition of KOH raises the amorphous character of polymer chains and diminishes the thermal stability of the PVA film [9]. Besides, the ionic conductivity of PVA-KOH polymer is highly influenced by the amount of KOH and H_2O molecules inside the membrane [9,20,21]. Ionic conductivity values of 4.7 10^{-2} S cm^{-1} have been reported for PVA-KOH films [9].

In addition, with the aim to improve their electrochemical and mechanical properties, PVA has been blended with others materials, such as polymers, crosslinking agents or chemically inert materials. [5,6,22–28]. For instance, ionic conductivity values of 2.2 10^{-1} S cm^{-1} have been reached for a PVA-KOH polymer cross-linked with poly (ethylene glycol) diglycidyl ether (PEGDGE) [27].

In this work, new results obtained for PVA-KOH hydrogels by several experimental techniques, such as XRD, TGA, XPS and ATR-FTIR, have

* Corresponding author.
E-mail address: antonioj.fernandez@upct.es (A.J. Fernández Romero).

https://doi.org/10.1016/j.jelechem.2019.113380
1572-6657/

demonstrated the polymer structural changes occurred in the polymer electrolyte depending on the amount of KOH and H_2O molecules added to the PVA. Besides, AC Impedance spectroscopy, cyclic voltammetry and Galvanostatic Discharge tests have evidenced the improvement of the ionic transport along the membrane depending on the amount of KOH and water in the film. Finally, XRD and EDX measurements demonstrate the confinement of Zn^{2+} close to Zn electrode during the test of Zn/Air batteries, making necessary the movement of OH^- anions inside the membrane, as the only ionic species causing the charge transport through the membrane. This fact, together with spectroscopic and electrical results allows us to discuss the improvement of the anionic transport inside the membranes based on the Grotthuss mechanism.

2. Material and methods

PVA MOWIOL 18–88 (MW 130.000), PVA 20–98 (MW 125.000), KCl (>99%), NaOH (>97%) and KOH (85%) were obtained from Sigma-Aldrich., Millipore water with resistivity of >18MΩcm was always used.

The preparation of the GPEs was carried out following the solution casting method. Briefly, PVA was dissolved in deionized water at 90 °C under severe stirring for two hours until a clear solution was obtained. Once the solution was cold, different volumes of KOH 6 M were dropwise added maintaining the stirring. The resulting liquid was then poured into a Petri dish and let to cast in controlled atmosphere to avoid the presence of carbon dioxide. After that, the membranes were kept in a desiccator until required for use. Specimens of 12 mm diameter were punched immediately before being tested in batteries and conductivity measurements.

Besides, PVA-KOH soaked membranes were obtained starting from specimens of PVA-KOH gels dried for 10 days, which subsequently were immersed in KOH 12 M for 24 h prior to be used in any test. The soak step was also carried out in absence of CO_2 into an atmosphere controlled desiccator. Before any test, all specimens soaked or not, were rinsed with plenty of water to remove the rest of KOH from the membrane surface.

Table 1 shows the initial weight of the components used in each prepared GPE. Membranes PVA-KOH 10, PVA-KOH 30 and PVA-KOH 50 have been obtained adding 10 ml, 30 ml or 50 ml of 6 M KOH solution to the PVA solution, respectively. Besides, membrane PVA-KOH 30 swollen (designed by PVA-KOH 30 sw) stand for a PVA-KOH 30 membrane, which was immersed in a 12 M KOH solution for 24 h.

X-ray diffraction patterns were collected using a computer-controlled Bruker D8 Advance laboratory diffractometer, operated in the reflection Bragg–Brentano geometry and configured in the θ/θ mode to maintain a horizontal sample position at all times. The data were collected at room temperature, using Cu-Kα (λ = 1.5418 Å).

XPS spectra were recorded using a hemispherical analyzer. Non-monochromatized Mg K_α (1253.6 eV) X-rays were used. The data are analyzed after removing the Mg K_α satellite lines, as well as subtracting a Shirley type background and charge referenced to CH_2 species of C 1s peak at 284.8 eV. Peak fitting of C ls and O 1s were performed using Gaussian line-shapes with a fixed FWHM of 1.8 eV and 2.1 eV, respectively.

SEM coupled with EDX analysis was carried out using a Hitachi S-3500 N scanning electron microscope (Hitachi High-Technologies Corporation, Tokyo, Japan), using 70 Pa chamber pressure for back-scattered electrons (BSE) or <1Pa for secondary electrons (SE). Microanalysis was done with a *XFlash 5010 Bruker AXS Microanalysis*, with a resolution of 129 eV.

ATR-FTIR spectra were obtained using a Thermo Nicolet 5700 Infrared Spectrometer in the wave number range from 400 cm^{-1} to 4000 cm^{-1}. Thermo-gravimetry analysis was done on samples of 5–10 mg using a Mettler-Toledo TGA/DSC 1HT up to 700 °C, at a heating rate of 10 °C/min and under N_2 atmosphere. Cyclic voltammetry was carried out using symmetric Zn/GPE/Zn cells by means of a Biologic VSP Modular 5 channels potentiostat/galvanostat.

Ionic conductivity was determined from AC impedance measurements using the same potentiostat/galvanostat in the frequency range from 100 kHz to 40 mHz. The temperature was set by a Julabo F25 thermostat in the range from 278 to 343 K. Two platinum electrodes of 1 cm^2 area were used, which acted as blocking electrodes.

Ionic conductivity, σ, was calculated from the equation:

$$\sigma = l/R_b A \quad (1)$$

Galvanostatic Discharges were performed at 20 mA using a Biologic VSP Modular 5 channels potentiostat/galvanostat. The contact area was always 1.1 cm^2 and stainless steel current collectors were used. The cathode used in the experiments was the Air E4B electrode supplied by Electric Fuel Ltd. Zn powder (98.7%) and Zn plates (99.97%) used as anode in these cells were purchased from Goodfellow and Española del Zinc S.A., respectively.

Polarization curves were carried out with a current scan technique included in EC-Lab® software of the Biologic VSP potentiostat/galvanostat. The intensity changed from 0 to 100 mA at 0.1 mAs-1 scan rate. Before performance a current scan the battery was maintained at open circuit voltage (OCV). Three consecutive current scans were registered.

2.1. Membrane weight change

It is well known that the chemical and physical properties of the hydrophilic membranes are affected by the water content. [9,20,21] Besides, PVA membranes undergo swelling but they can also lose water as a function of ambient temperature and relative humidity. This fact is an important drawback for their application in devices such as Zinc/Air batteries [29].

In order to check the changes with the time of the membrane water content, we have studied how membranes weight is modified with storage time at ambient temperature. Fig. 1A shows the weight changes of a PVA-KOH 30 membrane for 25 days. As it can be seen, the membrane suffers a quick dehydration process during the first 72 h, but, after that, the loss of water slows down until it reaches a steady state. Fig. 1A displays also the ionic conductivity changes occurring to a PVA-KOH membrane maintained at room ambient temperature. As can be seen, ionic conductivity values tend to a constant as it was observed for membrane weights.

With the aim of keeping reproducible conditions as much as possible for the experiments where water content could play a critical role, membranes were always used after storage for 10 days at ambient temperature, assuring in this way steady water content.

Besides, we have monitored the weight changes of PVA-KOH 30 soaked membranes, which were stored 10 days at ambient temperature and then left soaking for 24 h in a 12 M KOH solution. In this case, we observe a quasi-steady weight and ionic conductivity behavior for 20 days, from the beginning (Fig. 1B). Note that measurements for

Table 1
Initial weights of PVA and KOH used to prepare the membranes and Activation Energy, E_a, and Ionic Conductivity values, σ, obtained for each membrane.

MEMBRANE	m_{PVA} /g	m_{KOH} /g	E_a /eV	σ /Scm^{-1}
PVA PURE	4	0	-	$\approx 10^{-10}$ [33]
PVA-KOH 10	4	3.36	0,18	0.012
PVA-KOH 30	4	10.10	0.15	0.14
PVA-KOH 50	4	16.83	0.21	0.16
PVA-KOH 30 sw	4	10.10 + χ	0.16	0.34

χ is the additional amount of KOH incorporated into the membrane during the immersion of the membrane in 12 M KOH solution. Ionic conductivity values have been obtained at T = 20 °C.

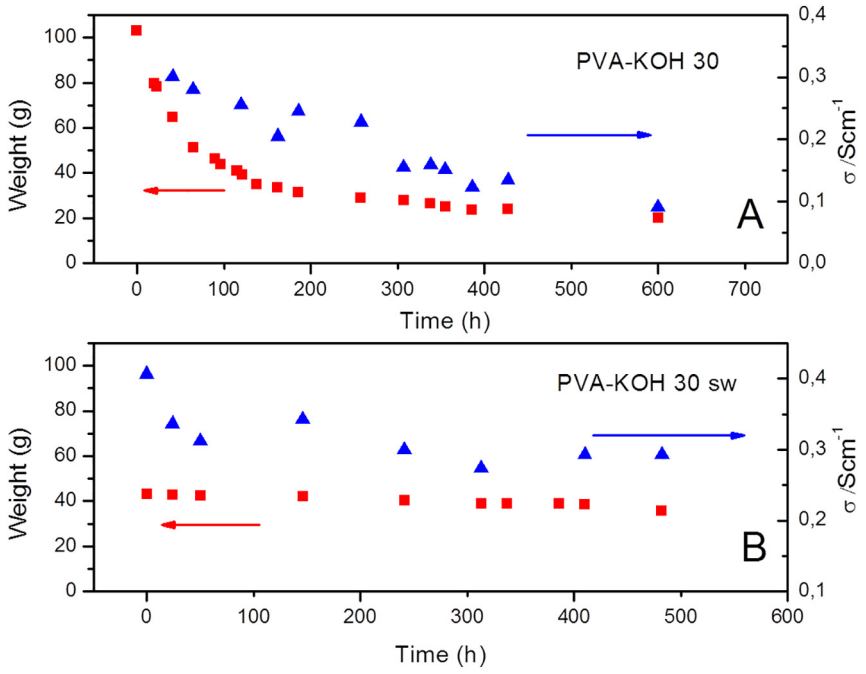

Fig. 1. Membranes weight and ionic conductivity values changes with the storage time at ambient temperature. A) For a PVA-KOH 30 membrane and B) For a PVA-KOH 30 swollen membrane.

soaked membrane start when the hydrogel was pulled out of the 12 M KOH solution, that is after 24 h immersed in this solution.

On the other hand, when a dry hydrophilic polymer, such as PVA, is dipped in water the interaction between water molecules and polymer chains provides an expansion of the polymer until reaching an equilibrium swelling level. The swelling behavior of hydrogels can be ascertained by different methods. We have calculated the swelling ratio (SR) following the next equation [5]:

$$SR = 100\ x\frac{m_e - m_d}{m_d} \quad (2)$$

where m_d and m_e are weights of samples before and after swelling, respectively. The immersion time in KOH 12 M was always 24 h. Table 2 shows the swelling values for five PVA-KOH 30 membranes. A SR value of 34 ± 2% was always obtained.

3. Results and discussion

3.1. Structural characterization of the gel polymer electrolytes

3.1.1. XRD

The X-ray diffractometry (XRD) is a useful tool to distinguish the different crystalline phases of PVA-KOH hydrogels [30,31]. Fig. 2 shows the XRD spectra of pure PVA as well as PVA-KOH membranes at different concentrations of KOH, which are very similar to those previously reported [30]. Besides, a PVA-KOH 30 swollen membrane is displayed.

Table 2
Swelling ratios for different PVA-KOH-30 membranes after their immersion for 24 h in KOH 12 M.

Sample	Initial weight /g	Weight after soaking /g	Swelling Ratio /%
A	0.93	1.23	32.26
B	0.75	1.00	33.33
C	0.76	1.02	34.21
D	0.73	0.99	35.62
E	0.78	1.03	32.05

The pure PVA pattern shows a big peak at 2θ = 20° and a secondary peak at 40.5°. These peaks indicate a certain extent of crystalline phase in pure PVA, which can be associated with polymer chains alignment due to H-bonds formed between OH groups of packed PVA chains. However, once the KOH solution is incorporated inside the polymer matrix, lower intensity and wider peaks are found in the XRD patterns, indicating an increase of the amorphous domains in the PVA structure [32]. Note that the PVA-KOH 30 sw membrane presents the lower intensity peaks.

These changes have to be provided by the retention of KOH and water molecules inside the polymer, which will be related to interactions between KOH, H_2O molecules and PVA chains.

3.1.2. XPS measurements

As can be seen in Fig. 3A for a PVA KOH 30 membrane, XPS peaks observed at 292.5 and 295.3 eV assigned to $K2p_{3/2}$ and $K2p_{1/2}$ demonstrate the presence of K inside the PVA-KOH GPE. Besides, C1s region is shown in this figure. The analysis of C1s core level shows a main peak at 284.8 eV attributed to CH_2 species of the polymeric chains, two small components at 286.5 and 287.8 eV assigned to C-OH [33] and carbonyl C═O species, respectively, and a more pronounced peak at 289.3 eV attributed to carboxylate –COO species [34]. The presence of this peak confirms the existence of acetate groups inside the polymer, which is expected because the PVA used in this work is not fully hydrolyzed, containing up to 12% acetate groups, as manufacturer datasheet indicates. Besides, a low binding energy component is also observed at 282.7 eV. This component indicates the interaction between a metal (K) and the carbon.

On the other hand, the O1s region obtained for the PVA-KOH GPE is displayed in Fig. 3B. Deconvolution of the O 1s spectra is complex due to the small differences in O ls binding energy for -OH, C═O, and C-O-C species, together with the broadness of the peaks [35]. O1s experimental peak has been fitted with three components at 528.9, 531.0 and 532.7 eV.

The main peak at 531.0 eV has been assigned to -OH, C═O, and H_2O species, without being able to distinguish between them. The peak at 532.7 eV can be assigned to the single bonded oxygen in the carboxylate –COO group, since this oxygen atom presents higher binding energy

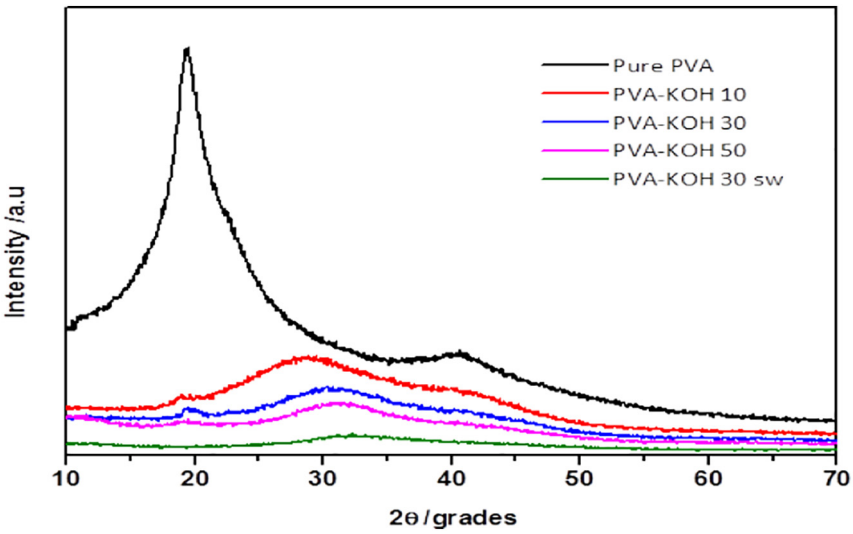

Fig. 2. XRD patterns of the prepared membranes.

than the oxygen atoms present in the -OH, C═O, and H_2O groups. [35]. Finally, the lower binding energy component observed at 528.9 eV has to be assigned to the interaction between O and a Metal (M-O). In this case, as only K metal is inside the polymer, this peak points to a K—O interaction and taking into account the low binding energy shoulder of the C 1s orbital, it is interesting to note the presence of K bonded to C and O. The presence of Metal-C-O complexes has been already reported in the literature for evaporated Aluminum on PVA [36].

3.1.3. Thermogravimetric analysis

Fig. 4 compares the thermos-gravimetric curves of pure PVA with PVA-KOH gel electrolytes. Initially, pure PVA presents a 10% weight loss, which is attributed to free water remaining in the membrane. A second weight loss proceeds quickly with onset at 310 °C and it involves two processes: elimination of side chains acetate groups and OH groups to produce polyenes [37,38]. At around 420 °C a third step is observed which has been assigned to PVA backbone breaking [37,38]. These three steps are clearly identified in the TGA derivative curve (inset in Fig. 4). At the end, only a 5% of initial weight of pure PVA remains.

With respect to PVA-KOH membranes, all of them have a mass loss at around 100 °C. However, the amount of water is higher with the quantity of KOH solution used during the synthesis process. A second weight loss is observed at around 200 °C, which will correspond to OH groups and side chains elimination. Finally, the third weight loss, corresponding to PVA backbone breaking, is observed at around 430–440 °C [37,38].

It should be noted that while the onsets observed for the first and the third steps are close for all membranes, the onset obtained for the second step for PVA-KOH membranes occur at 110 °C lower than the temperature obtained for pure PVA. Furthermore, the inclusion of KOH and water inside the membrane only affects the second step, which is related to the removal of OH groups and side chains of PVA. This fact indicates that KOH-H_2O included in the membrane interact with OH and carbonyl groups of the PVA chains. Thus, the thermal stability of the PVA system is diminished once the KOH-H_2O is incorporated to the

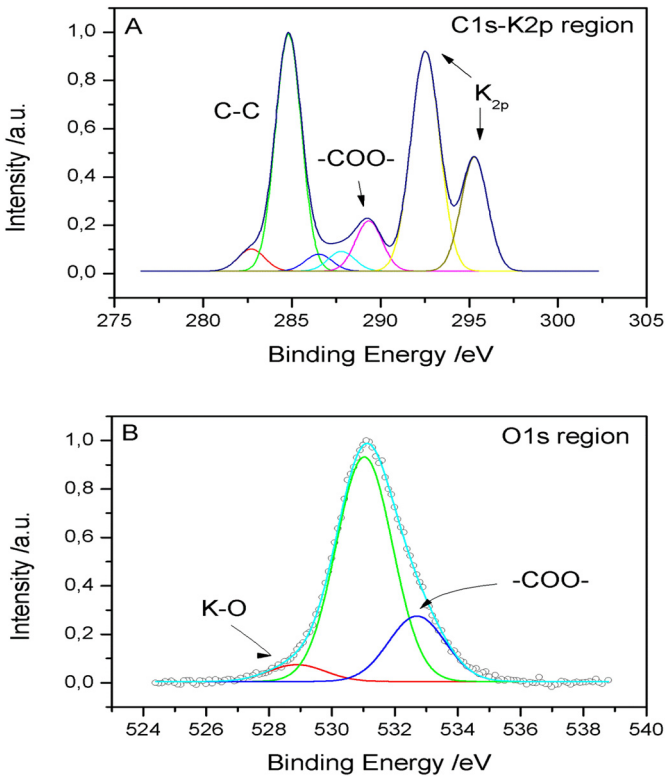

Fig. 3. XPS spectra of PVA-KOH 30 membrane. A) C1s and K2p region. B) O1s region.

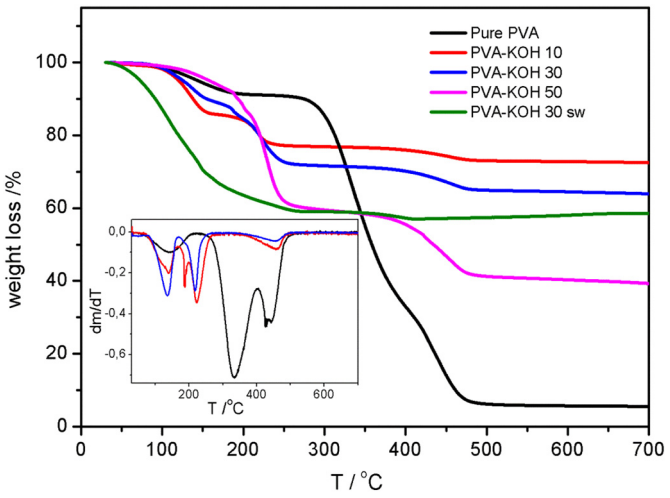

Fig. 4. TG curves of the prepared membranes. Inset shows the differentiated TG curves of PVA-KOH membranes.

gel [9]: it must disrupt somehow the interaction between OH groups of nearby polymer chains, making the new polymer structure weaker. This result is in agreement with the KOH interaction with PVA chains deduced from ATR-FTIR spectra, as it will be commented below. It is known that at higher water contents, water molecules weaken the hydrogen bonds between polymer chains and it leads to an increase in free volume [39].

This argument is again supported by the PVA-KOH 30 soaked membrane TGA results shown in Fig. 4, where the second step occurred at an even lower temperature. As can be seen, this curve is very different from those obtained from non-swollen membranes, pointing to a great structural change. At 100 °C there is a weight loss of 27%, indicating that this membrane presents a higher amount of water. At 150 °C, a change of slope is observed, which corresponds to OH and acetate groups elimination, confirming that membrane stability clearly decreases. Besides, a small step is observed near 400 °C. These results are in agreement with the crystallinity loss observed in XRD spectra when KOH is incorporated to PVA membranes: a more amorphous GPE has lower stability.

Finally, we have paid attention to the residue remaining at 700 °C for each membrane analyzed. For pure PVA membrane only 5% of the total weight remains, while those membranes including KOH present higher weight rest at 700 °C, which increases with the amount of KOH incorporated inside the membrane. This rest material should be related to the amount of potassium, which could form K_2O compound at these high temperatures, as it has been proposed before [40].

With respect to the PVA-KOH 30 swollen membrane, the residue remaining at 700 °C is 58.3%, which is lower than the percentage obtained for a similar non-swollen membrane, 63.9%. This apparent contradiction is explained considering the initial weight of both membranes and the swelling percentage for the PVA-KOH soaked membrane. Table 2 presents the initial and after swollen weight measured for 5 different samples of PVA-KOH 30 membranes. As can be seen, a 34 ± 2% swelling ratio has been always obtained. Considering the sample weights used in TGA analysis and the percentages remaining at 700 °C, we can calculate that non-swollen membranes hold 0.49 g of K compounds, while the swollen ones hold 0.59 g. From this calculation, we can conclude that during the swollen process more KOH, together with water molecules, has penetrated in the membrane from the KOH 12 M solution.

3.1.4. ATR-FTIR spectroscopy

In agreement with the XRD and TG results, introduction of KOH solution inside the membranes affects clearly the bands observed in the ATR-FTIR spectra (Fig. 5).

The pure PVA characteristic bands [41,42] can be observed in the ATR-FTIR spectrum shown in Fig. 5. Among them, bands at 1243, 1084, 945 and 1732–1710 cm^{-1} are attributed respectively to ν (C-O-C), ν (C—O), ν (C-C-O) and ν (C═O) modes due to the acetate groups remaining in the PVA structure from its manufacturing process. As it has been mentioned before, the presence of these bands is reasonable since 12% acetate groups are included in the PVA used, as the manufacturer datasheet indicates.

Conversely, when KOH is incorporated to PVA, several changes are found. Introduction of water molecules inside the polymer together with KOH is demonstrated by the 1640 cm^{-1} band, which appears in all spectra of PVA-KOH membranes, in agreement with KOH solution spectrum, included in Fig. 5. Besides, bands at 945, 1245 and 1732–1710 cm^{-1} assigned to acetate groups disappear. This behavior may be related to the hydrolysis of acetyl groups by OH^- groups of the KOH. However, in this case, peaks due to acetate groups should be observed in ATR-FTIR spectra although they were cleavaged from the PVA chains. On the other hand, XPS measurements have demonstrate the presence of C═O groups, which are due to acetate groups. In addition, several articles have reported the shift, diminution and/or disappearing of ~1740 cm^{-1} band of C═O groups, as a result of the interactions with cations or due to crosslinking of the PVA chains. [43–46]

Furthermore, the changes observed in the ATR-FTIR spectra point to interactions between KOH and PVA chains, as it was already deduced from XRD, XPS and TG measurements. Since oxygen atom in OH and C═O groups of the PVA is a strong electron donor due to it has lone pairs of electrons available, K^+ cations will be coordinated with these groups forming complex such as C═O···K^+ or C-O···K^+ These type of interactions has already been proposed for PVA doped with Mg^{2+} or Cd^{2+} salts [37,38]. XPS measurements confirm also this aspect (Fig. 3).

This interaction can be also checked out analyzing the 1084 cm^{-1} band observed for Pure PVA and assigned to ν (C—O). When KOH is incorporate to the membrane, this band diminishes their intensity and shifts at 1094, 1097 and 1099 cm^{-1} for PVA-KOH 10, 30 and 50 GPEs, confirming the C-O···K^+ interaction. In addition, a new peak observed at 1560 cm^{-1} appears in all GPEs doped with KOH, which can be assigned to carbonyl groups. A similar result has been already reported by J. Qiao et al. [5,46], who observed that introduction of KOH inside PVA-based membrane provided disappearance of the C═O peak observed at 1718 cm^{-1} while a new characteristic band centered at 1571 cm^{-1} appeared. These authors attributed this behavior to a disproportionation reaction of the "free" –CHO groups of the glutaraldehyde (GA) included in the membrane and assigned the 1571 cm^{-1} peak to the stretching vibration of the potassium carboxylate [C═O(-O-K)] formed. However, in this work we have not ever used GA as crosslinking agent. Thus, we can associate the band observed at 1560 cm^{-1} to the interaction between the acetate groups of the PVA and cations K^+.

On the other hand, important spectral changes are observed in the fundamental OH stretching region at 3000–3500 cm^{-1}. It has been frequently reported broader peaks and shifted to a lower wave number in this region when a higher quantity and stronger H-bonding are formed [47]. Hence, as it is observed in Fig. 5, PVA-KOH GPEs show shifts to lower frequencies and more broadness bands with the higher amount of KOH incorporated into the PVA. This result indicates that, though the inclusion of KOH solution inside the polymeric matrix provides the rupture of the inter chains H-bonds, a higher amount of H-bridges is formed with the increasing of KOH and H_2O molecules inside the GPE. Furthermore, a new H-bond network will be formed by PVA OH groups, water molecules and hydroxyl groups of KOH.

Fig. 5 also shows the spectrum of a PVA GPE doped with KCl, compared with those obtained for KOH-PVA 30 and Pure PVA. Surprisingly, the PVA-KCl spectrum is very similar to the one obtained for Pure PVA, although an intense 1640 cm^{-1} band is observed and the OH stretching band (in 3000–3500 cm^{-1} region) is more intense than the one

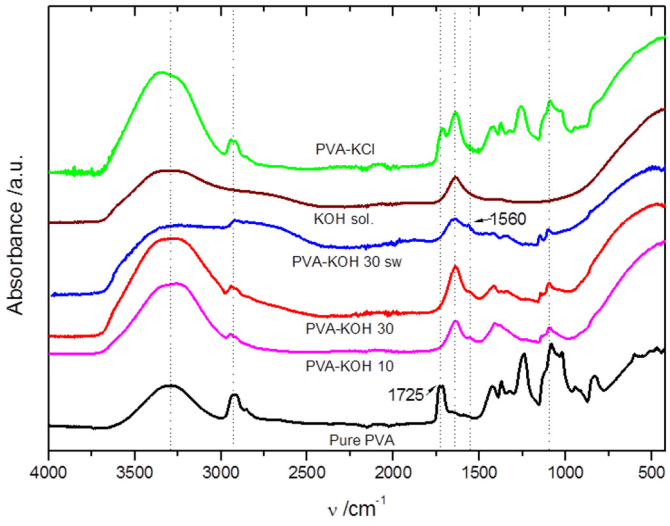

Fig. 5. ATR-FTIR spectra of the PVA Pure and PVA-KOH membranes. PVA-KOH sw denotes a PVA-KOH 30 membrane swollen in 12 M KOH for 24 h. Spectra of 6 M KOH solution and PVA-KCl 30 are included to compare.

obtained in pure PVA spectrum. Both facts can be explained by a higher amount of water molecules inside the PVA-KCl GPE. Besides, in this case all the pure PVA bands are observed in this spectrum with minimal intensity changes and shifted slightly. Among them, it has to be noted that the carbonyl band of acetyl groups is shifted until 1712 cm^{-1} and ν (C—O) mode is shifted to 1089 cm^{-1}. These shifts may indicate C=O···K+ and C-O···K^+ interaction, though weaker than those appearing in PVA-KOH. This result confirms that Cl^- anions have a small influence on the PVA chains compared with the hydroxyl groups of KOH.

Finally, we have also recorded an ATR-FTIR spectrum of a PVA-KOH 30 sw membrane, obtained by soaking a PVA-KOH-30 in KOH 12 M for 24 h (Fig. 5A). We found that the spectrum obtained does not show significant changes with respect to non-swollen membrane spectra. The same peaks obtained from the non-swollen membrane are observed in this case, except for wider bands at ≈3300 cm^{-1}, which has to be related to the incorporation of an additional amount of KOH and water inside the membrane, as it has already been deduced by XRD and TG measurements. Besides, 1560 cm^{-1} appeared and the ν (C—O) mode was shifted to 1102 cm^{-1}.

3.2. Electrical and electrochemical properties

3.2.1. Temperature dependence of ionic conductivity

Fig. 6A shows the variation of ionic conductivity with the temperature for PVA based GPEs with different concentration of KOH. All plots obey Arrhenius behavior throughout a wide temperature range, as it is

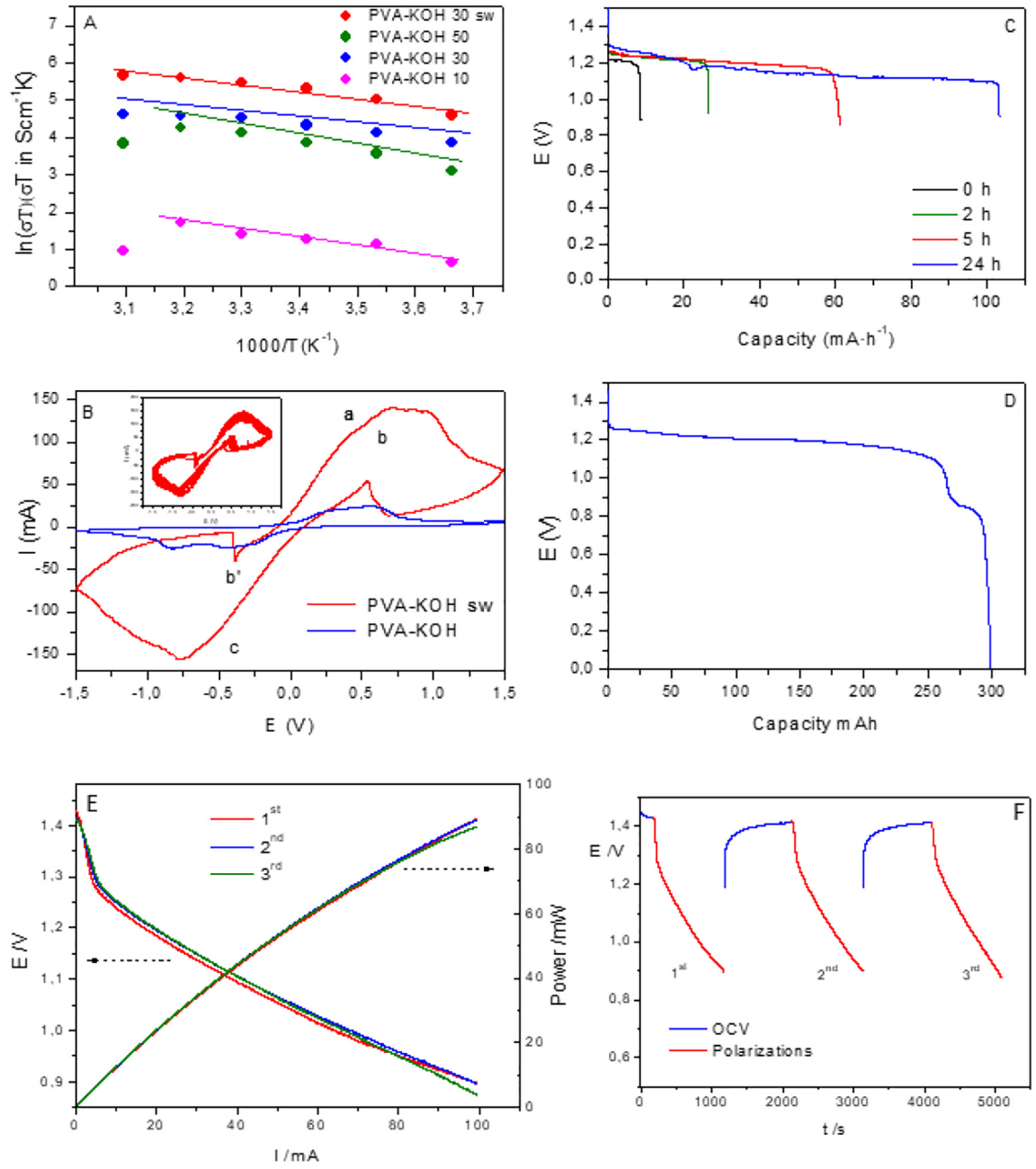

Fig. 6. A) Conductivity values of the PVA-KOH based membranes with the temperature, indicating an Arrhenius behavior. B) Cyclic Voltammograms of PVA-KOH 30 and PVA-KOH 30 swollen membranes. Inset: 50 consecutive cycles of the swollen membrane. C) Discharge curves of Zn/PVA-KOH 30/Air batteries with the immersion time of the PVA-KOH 30 membrane in 12 M KOH solution, using a Zn plate as anode. D) Discharge curve of a Zn/PVA-KOH 30 sw/Air, using Zn powder as anode. In this case, the PVA-KOH membrane was immersed 24 h in 12 M KOH solution. E) Polarization curves of a Zn/PVA-KOH 30 sw/Air battery at 0.1 mAs^{-1} scan rate. Three consecutive polarization curves were carried out after a OCV period. F) Potential versus time during the polarization measurements, including OCV and polarization curves.

confirmed by data fitted to the equation:

$$T = \sigma_0 \exp(-E_a/k_B T) \quad (3)$$

where σ_o is the pre-exponential factor, E_a the activation energy, k_B the Boltzmann constant and T the testing temperature. From slopes in Fig. 6A the activation energy values can be obtained, which are shown together with conductivity values at 20 °C for all membranes in Table 1. Lower E_a values of 0.15 ± 0.01 were obtained for PVA-KOH 30 and PVA-KOH 30 sw membranes, with respect to PVA-KOH 10 and PVA-KOH 50. As can be seen in this Figure and Table 1, similar ionic conductivity values of 0.15 ± 0.01 Scm^{-1} at 20 °C were obtained for PVA-KOH 30 and 50 GPEs, which are much higher than those resulted for PVA-KOH-10 membrane, 0.012 Scm^{-1}. However, the highest conductivity value, 0.34 Scm^{-1} at 20 °C, was obtained for PVA-KOH 30 sw hydrogel, confirming the relevance of soaking the PVA-KOH membranes in 12 M KOH solution.

Temperature dependence of PVA-KOH 30 sw membranes is also included in Fig. 6A. As can be seen, the soaking of the membrane in KOH obeys again Arrhenius behavior, but conductivity values notably increase with respect to those not soaked. Increase of conductivity values of swollen membranes has to be related with the entrance of an additional amount of KOH and water during the swollen process, as it has been confirmed by ATR-FTIR, TGA and XRD measurements.

3.2.2. Cyclic voltammetry

In order to confirm the ionic transport into the GPEs, a cyclic voltammetric (CV) study was carried out using a Zn/GPE/Zn symmetric cell. Fig. 6B shows the voltammetric behavior of PVA-KOH 30 and PVA-KOH 30 sw membranes. A huge increase of the current density is observed, which has to be associated with the effect of water and KOH uptake during the soaking process.

As can be seen, a quasi-reversible behavior is obtained for oxidation/reduction processes, with a and c peaks charges very closed. Besides, in the cathodic sweep a low anodic peak, b, is observed. This peak has been reported before, and it was assigned to the further oxidation of Zn after the dissolution of the passive film formed on the Zn electrode surface, which come off during the cathodic scan [48]. These authors use a convectional three electrode cell, with Pt as counter-electrode, and observed the peak b only in the cathodic branch of the voltammogram. However, we have used a Zn/PVA-KOH/Zn cell and this is the reason why we found this peak type, b and b', in both voltammetric branches.

Besides, the quasi-reversible behavior of the oxidation/reduction processes is demonstrated in the inset of Fig. 6B, where 50 consecutive cycles of the PVA-KOH soaked membrane are shown, confirming a very steady behavior with the cycling. This result corroborates the usefulness of this membrane type in rechargeable batteries.

CV results together with ionic conductivity and activation energy values confirm that these membranes should be good candidates to be used as gel polymer electrolytes in Zn-based batteries.

3.2.3. Zn/GPE/Air batteries

Electrochemical performance of Zn/PVA-KOH/Air batteries has been examined carried out by galvanostatic discharge profiles and polarization curves. With the aim of proving the usefulness of PVA-KOH membranes as polymer electrolytes, we have tested Zn/PVA-KOH/Air batteries at −5 mA discharge current, using a Zn plate as anode. As can be seen in Fig. 6C, non-soaked membrane provides a very low discharge capacity value, 7 mAh. However, discharge capacity values increase with the time the membrane was soaked in the 12 M KOH solution. Discharge capacities of 110 mAh were obtained for a PVA-KOH membrane soaked in 12 M KOH for 24 h.

Besides, a soaked PVA-KOH 30 membrane has been tested in a Zn/PVA-KOH/Air battery at room temperature, using a Zn powder anode instead of Zn plates. Fig. 6D shows the first discharge and charge curves carried out at −20 $mAcm^{-2}$, where discharge capacities of ~300 $mAhg^{-1}$ were obtained.

Additionally, polarization curves were accomplished from 0 to 100 mA at 0.1 mAs-1 current scan rate (Fig. 6E and F). Three consecutive scans were carried out after an open circuit voltage (OCV) period. Fig. 6E shows the repeatability of the potential versus intensity curves, obtained after OCV periods, where the same potential of 0.9 V at 100 mA was reaching in the three curves. Fig. 6F displays the potential versus time of the complete polarization measurement, where a OCV initial value of 1.43 V was obtained. As can be seen, after each polarization curve and a OCV period of 16 min this potential value was reached again, confirming the repeatability of the discharge curves.

Finally, we have confirmed that this kind of membranes can be used in rechargeable batteries. Two membranes used in discharge and discharge/charge processes have been analyzed by XRD (Fig. 7A). As it is

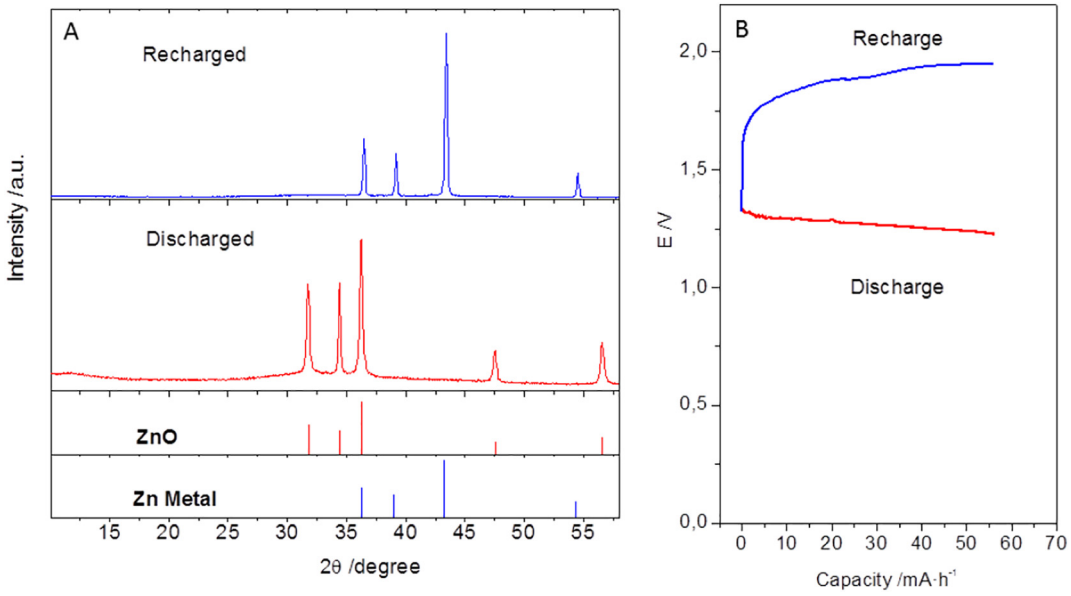

Fig. 7. A) XRD patterns of PVA-KOH membrane used in Zn/PVA-KOH 30 sw/Air batteries after a Discharge and a Discharge/Charge cycle curves of Zn/PVA-KOH 30/Air batteries. Vertical lines show the ICDD database cards of Zn [Card-00-004-0831] (blue) and ZnO [Card-00-036-1451] (red) B) Discharge and Charge curves of a Zn/PVA-KOH 30 sw/Air battery.

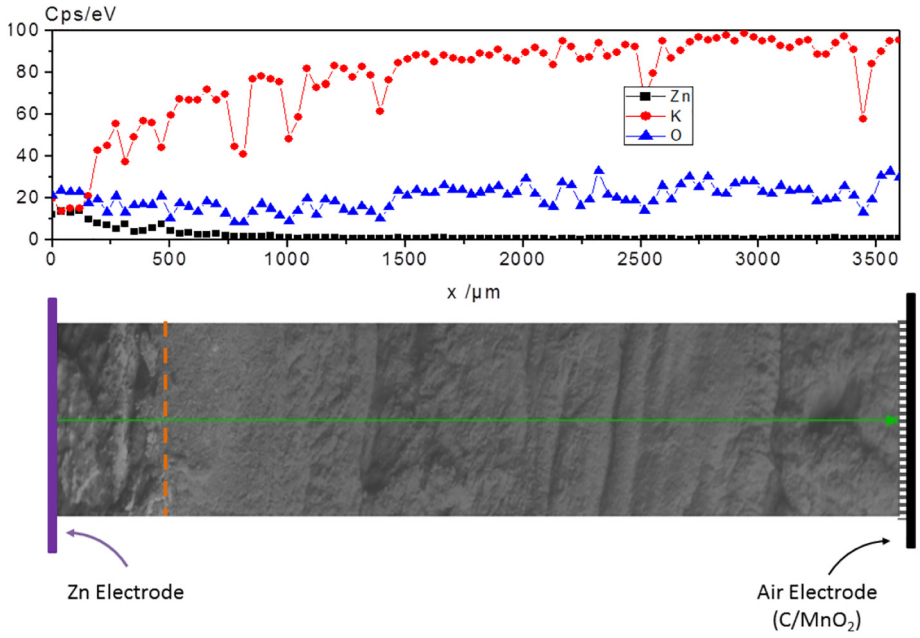

Fig. 8. SEM image and EDX line profile analysis of the cross section of a PVA-KOH 30 sw membrane used during a discharge in a Zn/PVA-KOH/Air battery. Zn, K, and O atoms were analyzed by EDX line profile from the membrane surface that was in contact with Zn electrode until reaching 3600 µm in depth.

shown, only ZnO is observed after a discharge process and only Zn Metal peaks appeared after a discharge/charge process, confirming that Zn Metal was oxidized forming ZnO during discharge and all Zn^{2+} cations were reduced to obtain again Zn Metal during the charge process. Note that the XRD analyses shown in Fig. 7 were carried out to PVA-KOH membranes, not to Zn electrodes. Fig. 7B shows the discharge and charge curves.

3.3. OH^- transport inside the PVA-KOH membranes

The alkaline PVA-based polymer electrolytes have shown ionic transport properties of anionic exchange membranes (AEM) with negative transport numbers, t_-, close to 1. Thus, C—C Yang et al. [28] reported t_- values ranging between 0.92 and 0.98 for PVA-KOH polymers, depending on the intensity applied and solution concentration used to carry out the t_- measurements by Hittorf's method. Besides, when tetraethyl-ammonium-chloride (TEAC) was incorporated to PVA-based membrane, t_- values of 0.99 were reached.

In this sense, we have obtained similar t_- values following an Evans method [11,17], but we have used two Zn electrode to obtain the anionic transfer number of PVA-KOH membranes. A 0.99 t_- value was obtained for PVA-KOH membranes soaked in KOH 12 M solution, confirming the OH^- anions as the only ionic species moving through the membrane.

With the aim to confirm if Zn^{2+} cations are moved through the membrane, we have carried out additional experimental measures. Fig. 8 shows a SEM image of the cross section of the PVA-KOH 30 membrane used during a discharge in a Zn/PVA-KOH/Air battery. Besides, we have carried out a EDX line profile analysis of Zn, K, and O from the membrane surface that was in contact with Zn electrode until reaching 3600 µm in depth. As can be seen, O amount is stable all along the membrane. However, K and Zn varies with the depth: K quantity is minimum near the Zn electrode ($x = 0$), but at $x = 150$ µm increase quickly until reaching a stable valor in the electrolyte bulk. Conversely, Zn is maximum close to Zn electrode, between $x = 0$ and $x = 100$ µm, after that it goes down slowly until $x = 500$ µm, where the amount of Zn^{2+} is zero. It should be noted that Zn atoms are confined to 0–500 µm zone and, beyond that Zn is not observed. Paying attention to the SEM image, a change of the membrane structure is clearly observed near 500 µm (this interface is marked with an orange line in the image). This result confirms that ZnO is formed close to Zn electrode surface and Zn^{2+} cations are not transported to the electrolyte bulk. As it is shown in XRD difractograms carried out on the PVA-KOH side in contact with the Zn electrode, ZnO peaks are observed in the PVA-KOH membrane after discharging process, but only Zn Metal peaks appear for the membrane used in a discharge and charge cycle (Fig. 7), confirming that this battery can be recharged.

Furthermore, the ionic transport is mainly anionic in our PVA-KOH membranes and thus, we can consider the OH^- as the only species contributing to the ionic transport inside the membrane.

Several transport mechanisms have been considered to participate in the OH^- transport through a membrane, such as diffusion, migration, convection or the Grotthuss mechanism. Although all of these mechanisms can participate in the OH^- transport, several authors assume OH^- is transported mainly following the Grotthuss mechanism at higher membrane water contains [6,21,49].

On the other hand, it is known that OH^- movement can be impeded by a closed structure of the polymer, as well as a strong interaction between OH^- and the polymer chains. It has been reported that OH^- transport inside the membrane clearly depends on the amount of water and KOH concentration included in the membrane and the pore sizes formed in the polymer structure [19–21]. It is reasonable to think that

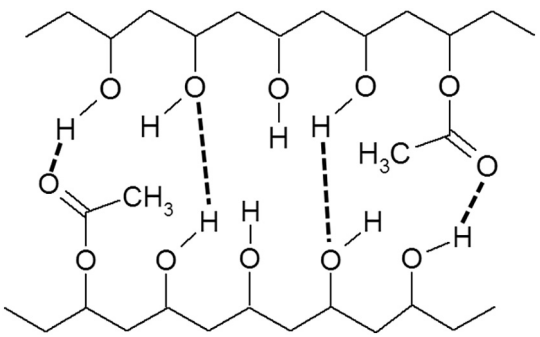

Scheme 1. Structure of a PVA membrane without KOH.

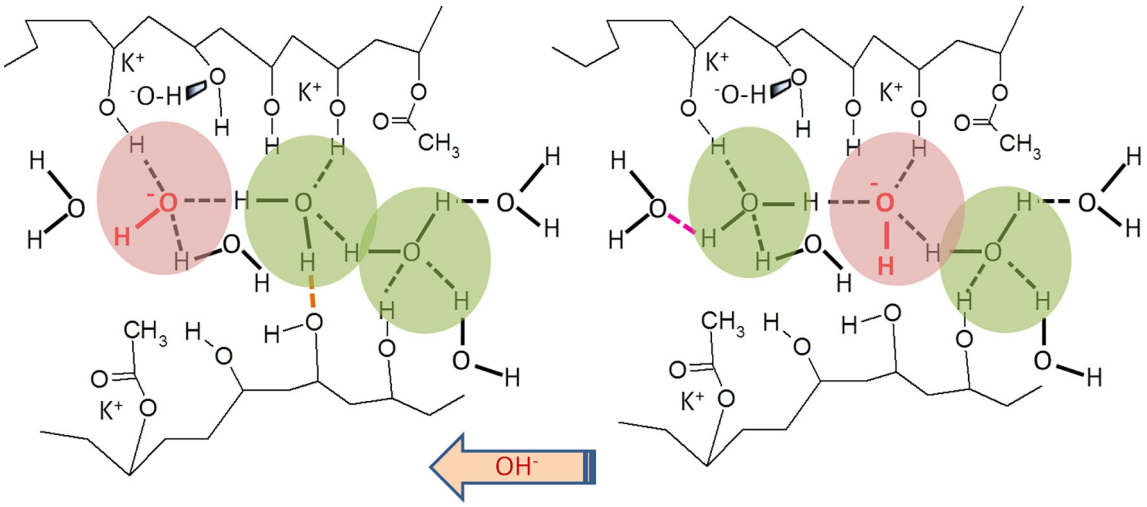

Scheme 2. OH^- transport following a Grotthuss Mechanism in a PVA-KOH 30 membrane. The arrow shows the OH^- transport direction. During the OH^- transport, a H-bond (pink) is broken and a new H-bond (orange) is formed.

greater pores will make easier the ionic movement, as it has been confirmed before. Besides, water amount influences the conductivity process in several ways: 1) A higher water uptake will increase the pore spaces between polymer chains and will decrease the strength of interaction of OH^- with the polymer chains. 2) Enough quantity of water inside the polymeric matrix is necessary to form an H-bonds network and to build up hydroxyl anions with stable solvation shells. 3) Finally, water molecules coming in the polymer matrix provide the decreasing of the crystalline phase to the benefit of the amorphous regions, enhancing the conductivity values of PVA-based membranes [6,21].

Regarding the PVA-KOH polymers synthesized in this work, we have observed by XRD measurements that the inclusion of KOH and water inside the PVA matrix provides an increase of the polymer amorphous regions, which will help to enhance the ionic conductivity. In addition, ATR-FTIR and TG measurements reveal interactions between PVA chains and the KOH and H_2O included in the polymer. These interactions are more important when a higher amount of KOH and H_2O are incorporated proving that immersion of PVA-KOH films in KOH 12 M solution, where additional KOH and H_2O are up-taken, provides the more important restructuration of the PVA chains.

Taking into account the above comments and our results, we can propose that the Grotthuss mechanism significantly contributes to or is the central mechanism for hydroxyl anion transport through PVA-KOH canals, though diffusion or migration cannot be completely discarded.

Furthermore, we propose here a tentative mechanism for the OH– transport inside the PVA-KOH membranes based on the Grotthuss theory.

Scheme 1 represents the PVA structure without KOH and H_2O. In this case, a great deal of Hydrogen bonds is formed between nearby PVA

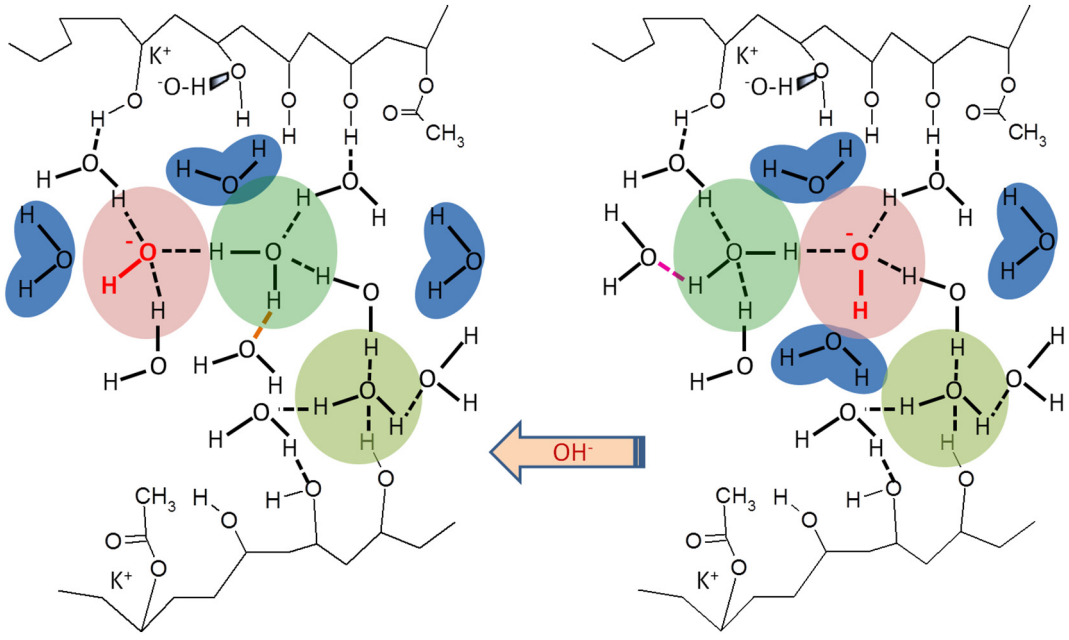

Scheme 3. OH^- transport following a Grotthuss Mechanism in a PVA-KOH 30 swollen membrane. The arrow shows the OH^- transport direction. During the OH^- transport, a H-bond (pink) is broken and a new H-bond (orange) is formed.

chains, making this structure very packed, which will prevent the ion movement. Thus, the ionic conductivity value of this polymer will be very low, as it is well known.

Conversely, the presence of KOH and H_2O in the PVA-KOH polymers breaks a great number of inter-chain H-bonds, though the modification of 3500 cm^{-1} reveals that a new H-Bond network is formed, probably including OH groups of the PVA chains, OH^- from the KOH and H_2O molecules. This process causes separation of the chains creating wider channels and making easier the movement of the OH^- anions. It should be noted that Grotthuss mechanism needs enough amount of H_2O molecules to form the solvation shell of the OH^- anions [6,21,49]. In this mechanism, OH^- solvated by four H_2O molecules, OH^--$(H_2O)_4$, are considered as inactive OH^- anions. They are transformed to active OH^--$(H_2O)_3$ solvation state, breaking an H-bond in the first solvation shell. In this state, the OH hydrogen forms an H-bond with another H_2O molecule, providing that the initial OH^- anion is now changed to an H_2O molecule tetrahedrally solvated, this is, a water molecule with an ideal bulk solvation pattern [6,21].

Schemes 2 and 3 show the Grotthuss mechanism occurring inside the PVA-KOH and PVA-KOH soaked in KOH 12 M, respectively. Both schemes show a similar OH^- transport through the PVA canals. However, in Scheme 2 the separation between PVA chains and the amount of KOH and H_2O inside the polymeric matrix will be lower than the one observed in Scheme 3. Thus, in non-soaked membranes, Scheme 2, a minor space inter PVA chains will cause that OH^- movement will be difficult and, probably the most of OH^- anions will create the solvation shell forming H-bonds with OH groups of the PVA chains and H_2O molecules. This fact will influence the OH^- transport inside the membrane, reducing the OH^- transport number and the ionic conductivity value with respect to soaked PVA-KOH membranes.

However, PVA-KOH membranes soaked in KOH 12 M solution, where a great deal of KOH and H_2O molecules were up-taken, will present a structure with a higher inter-chain space (Scheme 3). In this case, a higher number of OH^- anions will be able to develop complete solvation shells only with H_2O molecules without forming some H-bond with PVA OH groups. This situation will allow a faster transport of the OH^- anions through the polymeric canals. Furthermore, in this situation, higher ionic conductivity and anionic transport number values will be obtained, as it has been demonstrated by our results.

4. Conclusions

Different pure PVA and PVA-KOH membranes have been obtained by a solution cast method and they have been analyzed by several experimental techniques and applied as a polymer electrolyte in Zn/PVA-KOH/Air batteries. XRD, ATR-FTIR and TGA techniques have confirmed the restructuration of the PVA chains when KOH aqueous solution was included in the membrane. Besides, when these membranes are swollen in 12 M KOH aqueous solution a higher quantity of KOH and H_2O molecules are incorporated into the membrane, enhancing the polymer structure changes.

Soaking the KOH-PVA membranes in 12 M KOH aqueous solution improves the ionic transport properties: ionic conductivity of 0.34 Scm^{-1} and energy activation of 0.16 eV at room temperature were obtained. Besides, an increment of peak intensities of the voltammograms and larger capacity values in Zn/PVA-KOH/Air batteries resulted.

The improvement of this ionic transport behavior has been explained in the basis of the increase of the PVA inter-chains canals, a higher degree of *amorphosity* in the host polymer and the formation of a H-bond network, all of that motivated by the rise of KOH and H_2O inside the membranes. Finally, transport number of OH^- anions and the confinement of Zn^{2+} close to Zn electrode surface make necessary the OH^- anions transport through the membrane as the only ionic species causing conductivity, which may be explained by a Grotthuss mechanism.

Acknowledgements

The authors thank the financial support from Spanish Ministerio de Economía y Competitividad and AEI/FEDER/UE (Spain, Refs. ENE2016-79282-C5-5-R) and Fundación Séneca (Región de Murcia, Spain; Ref: 20985/PI/18).

References

[1] B. Scrosati, Applications of Electroactive Polymers, 3rd ed. Chapman and Hall, London, 1993.
[2] A.M. Stephan, Review on gel polymer electrolytes for lithium batteries, Eur. Polym. J. 42 (2006) 21–42, https://doi.org/10.1016/j.eurpolymj.2005.09.017.
[3] N.A. Choudhury, S. Sampath, A.K. Shukla, Hydrogel-polymer electrolytes for electrochemical capacitors: an overview, Energy Environ. Sci. 2 (2009) 55–67, https://doi.org/10.1039/B811217G.
[4] H. Inoue, in: G. Kreysa, K. Ota, R.F. Savinell (Eds.), Hydrogel Electrolyte. In Encyclopedia of Applied Electrochemistry, Springer NY 2014, pp. 1035–1039, https://doi.org/10.1007/978-1-4419-6996-5_515.
[5] J. Fu, J. Qiao, H. Lv, J. Ma, X.-Z. Yuan, H. Wang, Alkali doped poly (vinyl alcohol) (PVA) for anion-exchange membrane fuel cells-ionic conductivity, chemical stability and FT-IR characterizations, ECS Trans. 25 (2010) 15–23, https://doi.org/10.1149/1.3315169.
[6] G. Merle, M. Wessling, K. Nijmeijer, Anion exchange membranes for alkaline fuel cells: a review, J. Membr. Sci. 377 (2011) 1–35, https://doi.org/10.1016/j.memsci.2011.04.043.
[7] Z.S. Mahmud, N.H.M. Zaki, R.H.Y. Subban, A.M.M. Ali, M.Z.A. Yahya, MG49-KOH-PC alkaline gel polymer electrolytes membrane for supercapacitors, IEEE Colloquium on Humanities, Science and Engineering (CHUSER), Kota Kinabalu 2012 (2012) 621–626, https://doi.org/10.1109/CHUSER.2012.6504387.
[8] B. Li, X. Lu, J. Yuan, Y. Zhu, L. Li, Alkaline poly (vinyl alcohol)/poly (acrylic acid) polymer electrolyte membrane for Ni-MH battery application, Ionics 21 (2014) 141–148, https://doi.org/10.1007/s11581-014-1145-9.
[9] C.C. Yang, S.J. Lin, Preparation of composite alkaline polymer electrolyte, Mater. Lett. 57 (2002) 873–881, https://doi.org/10.1016/S0167-577X(02)00888-1.
[10] P.B. Bhargav, V.M. Mohan, A.K. Sharma, V.V.R.N. Rao, Structural and electrical properties of pure and NaBr doped poly (vinyl alcohol) (PVA) polymer electrolyte films for solid state battery applications, Ionics 13 (2007) 441–446, https://doi.org/10.1007/s11581-007-0130-y.
[11] J.P.T. Guisao, A.J. Fernández Romero, Interaction between Zn2+ cations and N-methyl-2-pyrrolidone in ionic liquid-based gel polymer electrolytes for Zn batteries, Electrochim. Acta 176 (2015) 1447–1453, https://doi.org/10.1016/j.electacta.2015.07.132.
[12] B. Scrosati, C.A. Vincent, Polymer electrolytes: the key to lithium polymer batteries, MRS Bull. 25 (2000) 28–30, https://doi.org/10.1557/mrs2000.15.
[13] S.-H. Wang, P.-L. Kuo, C.-T. Hsieh, H. Teng, Design of poly (acrylonitrile)-based gel electrolytes for high-performance lithium ion batteries, ACS Appl. Mater. Interfaces 6 (2014) 19360–19370, https://doi.org/10.1021/am505448a.
[14] W. Li, Y. Pang, J. Liu, G. Liu, Y. Wang, Y. Xia, A PEO-based gel polymer electrolyte for lithium ion batteries, RSC Adv. 7 (2017) 23494–23501, https://doi.org/10.1039/C7RA02603J.
[15] J.P. Tafur, A.J. Fernández Romero, Electrical and spectroscopic characterization of PVdF-HFP and TFSI-ionic liquids-based gel polymer electrolyte membranes. Influence of ZnTf2 salt, J. Membr. Sci. 469 (2014) 499–506, https://doi.org/10.1016/j.memsci.2014.07.007.
[16] J. Abad, F. Santos, J.P. Tafur, A. Urbina, E. Román, J.F. González-Martínez, J. Rubio-Zuazo, G.R. Castro, A.J. Fernández Romero, A synchrotron X-ray diffraction and hard X-ray photoelectron spectroscopy study of Zn negative electrodes at different charge and discharge states of Zn/MnO 2 batteries using an ionic liquid-based gel polymer electrolyte, J. Power Sources 363 (2017) 199–208, https://doi.org/10.1016/j.jpowsour.2017.07.082.
[17] J.P. Tafur, F. Santos, A.J. Fernández Romero, Influence of the ionic liquid type on the gel polymer electrolytes properties, Membranes 5 (2015) 752–771, https://doi.org/10.3390/membranes5040752.
[18] T.-Y. Wu, W.-B. Li, C.-W. Kuo, C.-F. Chou, J.-W. Liao, H.-R. Chen, C.-G. Tseng, Study of poly (methyl methacrylate)-based gel electrolyte for electrochromic device, Int. J. Electrochem. Sci. 8 (2013) 10720–10732.
[19] J.P. Tafur, J. Abad, E. Román, A.J. Fernández Romero, Charge storage mechanism of MnO_2 cathodes in Zn/MnO_2 batteries using ionic liquid-based gel polymer electrolytes, Electrochem. Commun. 60 (2015) 190–194, https://doi.org/10.1016/j.elecom.2015.09.011.
[20] A. Lewandowski, K. Skorupska, J. Malinska, Novel poly (vinyl alcohol)-KOH-H2O alkaline polymer electrolyte, Solid State Ionics 133 (2000) 265–271, https://doi.org/10.1016/S0167-2738(00)00733-5.
[21] K.N. Grew, W.K.S. Chiu, A dusty fluid model for predicting hydroxyl anion conductivity in alkaline anion exchange membranes, J. Electrochem. Soc. 157 (2010) B327–B337, https://doi.org/10.1149/1.3273200.
[22] W.H. Philipp, L.C. Hsu, Three Methods for In Situ Cross-Linking of PolyvinylAlcohol Films for Application as Ion-Conducting Membranes in Potassium Hydroxide Electrolyte. NASA Tech. Pap., No. 1407, 1979.
[23] K.C.S. Figueiredo, T.L.M. Alves, C.P. Borges, Poly (vinyl alcohol) films crosslinked by glutaraldehyde under mild conditions, J. Appl. Polym. Sci. 111 (2009) 3074–3080, https://doi.org/10.1002/app.29263.
[24] A.K. Sonker, K. Rathore, R.K. Nagarale, V. Verma, Crosslinking of polyvinyl alcohol (PVA) and effect of crosslinker shape (aliphatic and aromatic) thereof, J. Polym. Environ. 26 (2018) 1782–1794, https://doi.org/10.1007/s10924-017-1077-3.

[25] X. Liu, Q. Chen, L. Lv, X. Feng, X. Meng, Preparation of transparent PVA/TiO2 nanocomposite films with enhanced visible-light photocatalytic activity, Catal. Commun. 58 (2015) 30–33, https://doi.org/10.1016/j.catcom.2014.08.032.
[26] S. Sugumaran, C.S. Bellan, M. Nadimuthu, Characterization of composite PVA–Al2O3 thin films prepared by dip coating method. Iran, Polym. J. 24 (2015) 63–74, https://doi.org/10.1007/s13726-014-0300-5.
[27] G. Merle, S.S. Hosseiny, M. Wessling, K. Nijmeijer, New cross-linked PVA based polymer electrolyte membranes for alkaline fuel cells, J. Membr. Sci. 409-410 (2012) 191–199, https://doi.org/10.1016/j.memsci.2012.03.056.
[28] C.C. Yang, S.J. Lin, G.M. Wu, Study of ionic transport properties of alkaline poly (vinyl) alcohol-based polymer electrolytes, Mater. Chem. Phys. 92 (2005) 251–255, https://doi.org/10.1016/j.matchemphys.2005.01.022.
[29] Y. Li, H. Dai, Recent advances in zinc-air batteries, Chem. Soc. Rev. 43 (2014) 5257–5275, https://doi.org/10.1039/C4CS00015C.
[30] A.A. Mohamad, N.S. Mohamed, M.Z.A. Yahya, R. Othman, S. Ramesh, Y. Alias, A. Arof, Ionic conductivity studies of poly (vinyl alcohol) alkaline solid polymer electrolyte and its use in nickel-zinc cells, Solid State Ionics 156 (2003) 171–177, https://doi.org/10.1016/S0167-2738(02)00617-3.
[31] C.C. Yang, Chemical composition and XRD analyses for alkaline composite PVA polymer electrolyte, Mater. Lett. 58 (2004) 33–38, https://doi.org/10.1016/S0167-577X(03)00409-9.
[32] C.C. Yang, Study of alkaline nanocomposite polymer electrolytes based on PVA-ZrO2-KOH, Mater. Sci. Eng., B 131 (2006) 256–262, https://doi.org/10.1016/j.mseb.2006.04.036.
[33] P. Louette, F. Bodino, J.-J. Pireaux, Poly (vinyl alcohol) (PVA) XPS reference core level and energy loss spectra, Surf. Sci. Spectra 12 (2005) 106, https://doi.org/10.1116/11.20050922.
[34] S. Akhter, K. Allan, D. Buchanan, J.A. Cook, A. Campion and J.M. White, XPS and IR study of X-ray induced degradation of PVA polymer film, Appl. Surf. Sci.. 35 (1988–89) 241–258. doi:https://doi.org/10.1016/0169-4332(88)90053-0.
[35] D.T. Clark, B.J. Cromarty, A. Dilks, A theoretical investigation of molecular core binding and relaxation energies in a series of oxygen-containing organic molecules of interest in the study of surface oxidation of polymers, J. Polym. Sci. 16 (1978) 3173–3184, https://doi.org/10.1002/pol.1978.170161212.
[36] P. Stoyanov, S. Akhtert, J.M. White, XPS study of metal/polymer interaction evaporated aluminum on polyvinyl alcohol polymer, Surf. Interface Anal. 15 (1990) 509–515, https://doi.org/10.1002/sia.740150903.
[37] J.W. Gilman, D.L. Vanderhart, T. Kashiwagi, Thermal decomposition chemistry of poly (vinyl alcohol), Fire Polym. II Mater. Test Hazard Prev. 599 (1995) 161–185, https://doi.org/10.1021/bk-1995-0599.ch011.
[38] I. Restrepo, C. Medina, V. Meruane, A. Akbari-Fakhrabadi, P. Flores, S. Rodríguez-Llamazares, The effect of molecular weight and hydrolysis degree of poly (vinyl alcohol)(PVA) on the thermal and mechanical properties of poly (lactic acid)/PVA blends, Polimeros 28 (2018) 169–177, https://doi.org/10.1590/0104-1428.03117.
[39] R. Zelkó, G. Szakonyi, The effect of water on the solid state characteristics of pharmaceutical excipients: molecular mechanisms, measurement techniques, and quality aspects of final dosage form, Int. J. Pharm. Investig. 2 (2012) 18, https://doi.org/10.4103/2230-973X.96922.
[40] C.A. Strydom, A.C. Collins, J.R. Bunt, The influence of various potassium compound additions on the plasticity of a high-swelling south African coal under pyrolyzing conditions, J. Anal. Appl. Pyrolysis 112 (2015) 221–229, https://doi.org/10.1016/j.jaap.2015.01.023.
[41] J.E. Mark, Physical Properties of Polymers Handbook, Springer-Verlag Ed, New York, 2007 (https://doi.org/10.107/978-0-387-59002-5).
[42] Clariant GmbH. Mowiol Polyvinyl Alcohol1999.
[43] V.C. Costa, H.S. Costa, W.L. Vasconcelos, M.D.M. Pereira, R.L. Oréfice, H.S. Mansur, Preparation of hybrid biomaterials for bone tissue engineering, Mater. Res. 10 (2007) 21–26, https://doi.org/10.1590/S1516-14392007000100006.
[44] R.F. Bhajantri, V. Ravindrachary, A. Harisha, V. Crasta, S.P. Nayak, B. Poojary, Microstructural studies on BaCl2 doped poly (vinyl alcohol), Polymer 47 (2006) 3591–3598, https://doi.org/10.1016/j.polymer.2006.03.054.
[45] B.M. Baraker, B. Lobo, Spectroscopic analysis of CdCl2 doped PVA–PVP blend films, Can. J. Phys. 95 (2017) 738–747, https://doi.org/10.1139/cjp-2016-0848.
[46] J. Qiao, J. Fu, R. Lin, J. Ma, J. Liu, Alkaline solid polymer electrolyte membranes based on structurally modified PVA/PVP with improved alkali stability, Polymer 51 (2010) 4850–4859, https://doi.org/10.1016/j.polymer.2010.08.018.
[47] M. Reichenbächer, J. Popp, Challenges in Molecular Structure Determination. Vibrational Spectroscopy, Springer, Ed, 2012 108, https://doi.org/10.1007/978-3-642-24390-5.
[48] M. Cai, S.-M. Park, Spectroelectrochemical studies on dissolution and passivation of zinc electrodes in alkaline solutions, J. Electrochem. Soc. 143 (1996) 2125–2131.
[49] M.E. Tuckerman, D. Marx, M. Parinello, The nature and transport mechanism of hydrated hydroxide ions in aqueous solution, Nature 417 (2002) 925–929, https://doi.org/10.1038/nature00797.